

Article

Trimetallic Chalcogenide Species: Synthesis, Structures, and Bonding

 Sourav Kar ^{1,†} , Debipada Chatterjee ^{1,†} , Jean-François Halet ^{2,*}  and Sundargopal Ghosh ^{1,*} 
¹ Department of Chemistry, Indian Institute of Technology Madras, Chennai 600036, India

² Laboratory for Innovative Key Materials and Structures (LINK), IRL 3629, CNRS-Saint-Gobain-NIMS, National Institute for Materials Science (NIMS), Tsukuba 305-0044, Japan

* Correspondence: jean-francois.halet@univ-rennes1.fr (J.-F.H.); sghosh@iitm.ac.in (S.G.)

† These authors contributed equally to this work.

Abstract: In an attempt to isolate boron-containing tri-niobium polychalcogenide species, we have carried out prolonged thermolysis reactions of $[\text{Cp}^*\text{NbCl}_4]$ ($\text{Cp}^* = \eta^5\text{-C}_5\text{Me}_5$) with four equivalents of $\text{Li}[\text{BH}_2\text{E}_3]$ ($\text{E} = \text{Se}$ or S). In the case of the heavier chalcogen (Se), the reaction led to the isolation of the tri-niobium cubane-like cluster $[(\text{NbCp}^*)_3(\mu_3\text{-Se})_3(\text{BH})(\mu\text{-Se})_3]$ (**1**) and the homocubane-like cluster $[(\text{NbCp}^*)_3(\mu_3\text{-Se})_3(\mu\text{-Se})_3(\text{BH})(\mu\text{-Se})]$ (**2**). Interestingly, the tri-niobium framework of **1** stabilizes a selenaborate $\{\text{Se}_3\text{BH}\}^-$ ligand. A selenium atom is further introduced between boron and one of the selenium atoms of **1** to yield cluster **2**. On the other hand, the reaction with the sulfur-containing borate adduct $[\text{LiBH}_2\text{S}_3]$ afforded the trimetallic clusters $[(\text{NbCp}^*)_3(\mu\text{-S})_4\{\mu\text{-S}_2(\text{BH})\}]$ (**3**) and $[(\text{NbCp}^*)_3(\mu\text{-S})_4\{\mu\text{-S}_2(\text{S})\}]$ (**4**). Both clusters **3** and **4** have an Nb_3S_6 core, which further stabilizes $\{\text{BH}\}$ and mono-sulfur units, respectively, through bi-chalcogen coordination. All of these species were characterized by $^{11}\text{B}\{^1\text{H}\}$, ^1H , and $^{13}\text{C}\{^1\text{H}\}$ NMR spectroscopy, mass spectrometry, infrared (IR) spectroscopy, and single-crystal X-ray crystallography. Moreover, theoretical investigations revealed that the triangular Nb_3 framework is aromatic in nature and plays a vital role in the stabilization of the borate, borane, and chalcogen units.

Keywords: aromaticity; boron; cubane; selenium; sulfur



Citation: Kar, S.; Chatterjee, D.; Halet, J.-F.; Ghosh, S. Trimetallic Chalcogenide Species: Synthesis, Structures, and Bonding. *Molecules* **2022**, *27*, 7473. <https://doi.org/10.3390/molecules27217473>

Academic Editor: Roman Dembinski

Received: 6 September 2022

Accepted: 27 October 2022

Published: 2 November 2022

Publisher's Note: MDPI stays neutral with regard to jurisdictional claims in published maps and institutional affiliations.



Copyright: © 2022 by the authors. Licensee MDPI, Basel, Switzerland. This article is an open access article distributed under the terms and conditions of the Creative Commons Attribution (CC BY) license (<https://creativecommons.org/licenses/by/4.0/>).

1. Introduction

Metal-metal bonding is a constantly growing and widely studied area of chemistry [1–4]. The presence of d-orbitals in transition metals endows a much more diverse structure, chemistry, and chemical bonding than non-metal elements [5]. Paired metals can be linked by single [1,6–8], double [1,9], triple [9,10], quadruple [11], and in a few cases, quintuple bonds [12,13]. These types of metal–metal bonds are formed through σ , π , and δ -bonding interactions. With the exception of multiple bonding, metal atoms can form different types of frameworks, such as triangular, square, and three-dimensional clusters [14–20]. These metal frameworks (Chart 1) can show various types of aromaticity, such as σ -, π -, and δ -type. Recent findings of aromaticity in metal clusters have advanced the description of the electronic structures, chemical bonding, and stability of transition-metal clusters [21–27]. However, aromatic metal clusters are often observed in the gas phase, with the exception of a few cases [28,29]. For example, Robinson et al. structurally characterized the first ever main-group metal 6-electron aromatic cluster (see A in Chart 1) with π -aromatic properties, in 1995 [30]. Later, Maestri et al. isolated the transition-metal containing 2-electron π -aromatic cluster, namely $[\{\text{Pd}(\text{PPh}_3)(\text{SPh})\}_3]^+$ (C, Chart 1) [31]. On the other hand, Sadighi et al. isolated a 2-electron tri-gold monocation (B, Chart 1) showing σ -aromaticity [32]. Freitag et al. enriched a series of 2-electron σ -aromatic metal clusters with the isolation of the triangular clusters $[\text{Zn}_3\text{Cp}^*_3]^+$ (D, Chart 1) and $[\text{Zn}_2\text{CuCp}^*_3]$ [33]. Recently, Liddle et al. synthesized a 2-electron tri-thorium cluster $[\{\text{Th}(\eta^8\text{-C}_8\text{H}_8)(\mu\text{-Cl})_2\}_3\{\text{K}(\text{THF})_2\}_2]_\infty$ (E, Chart 1) with σ -aromatic metal-metal bonding [34]. These types of unique bonding

and aromaticity of metal frameworks may lead to the stabilization of many main group unstable species.

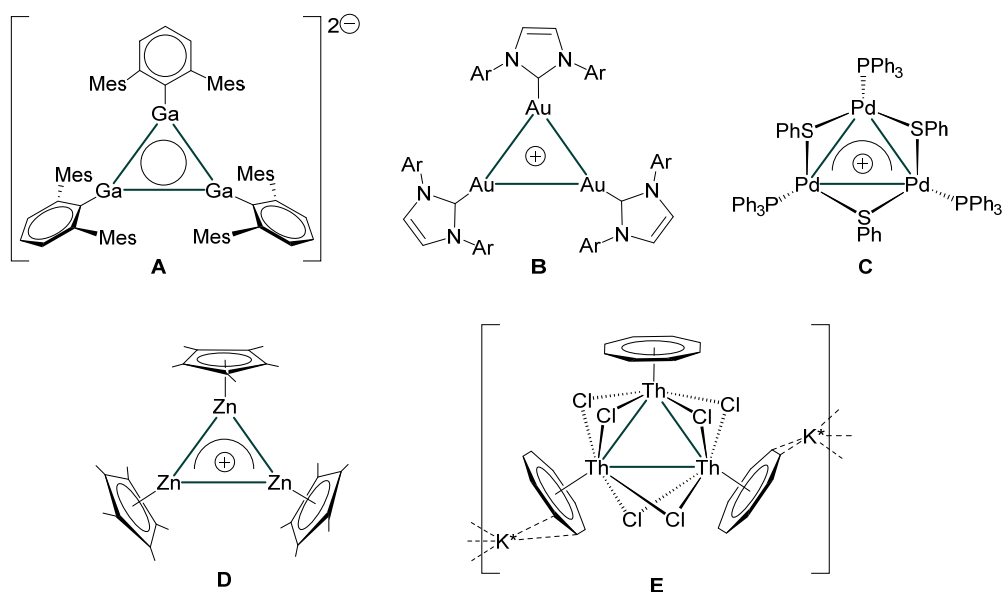


Chart 1. Different types of σ - and π -aromatic trimetallic clusters ((A): $[\text{Ga}(\text{Mes}_2\text{C}_6\text{H}_3)]_3^{2-}$, (B): $[(\text{IDipp})\text{Au}]_3^+$, (C): $[\{\text{Pd}(\text{PPh}_3)(\text{SPh})\}_3]^+$, (D): $[\text{Zn}_3\text{Cp}^*_3]^+$, (E): $[\{\text{Th}(\eta^8\text{-C}_8\text{H}_8)(\mu\text{-Cl})_2\}_3\{\text{K}(\text{THF})_2\}_2]_\infty$; Ar = 2,6-*i*Pr₂C₆H₃, IDipp = 1,3-bis(2,6-diisopropylphenyl)imidazol-2-ylidene, K* = K(THF)₂).

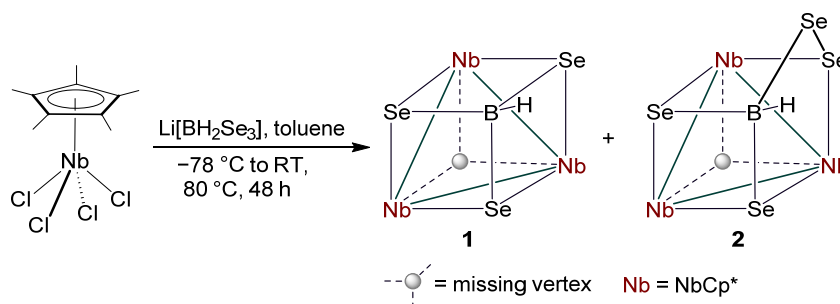
Many main group species that are quite unstable and not experimentally achieved as free species are isolated utilizing different types of metal frameworks [7,35–38]. For example, borylenes (B-R) can only be trapped by mono, bi, or tri-metallic frameworks [7,35]. In addition, many boranes and their analogues, from small boranes to higher nuclearity clusters, are stabilized in the coordination sphere of metals with structural and bonding diversity [7,14,36,39–43]. For example, we have recently isolated diborene(2) and diborane(4) utilizing group six trimetallic and bimetallic skeletons, respectively [44]. The first ever classical diborane(5) was also isolated utilizing a bimetallic coordination sphere of Ta atoms [45]. Further, a di-titanium framework allowed us to isolate the unique structural motif of hexa-borane $[\text{B}_6\text{H}_6]$, i.e., a hexagonal flat borane ring [8]. With the exception of borane, many other main group species are isolated utilizing metal's coordination sphere [46–49]. Further, we and others have isolated a series of group five trimetallic systems, which enabled us to isolate the thioborate ligand $\{\text{BS}_3\text{H}\}^-$ and its analogues [50–54]. In order to isolate small borane/borate and chalcogen species, we have extended our studies with niobium metal and heavier chalcogens. Herein, we present and discuss the isolation and structural explication of various trimetallic polychalcogenide frameworks, which stabilized tri/tetra-coordinated boron species and monochalcogen species. Theoretical calculations revealed the stability, bonding, and aromaticity of these trimetallic species.

2. Results and Discussion

2.1. Reactivity of $[\text{Cp}^*\text{NbCl}_4]$ with $\text{Li}[\text{BH}_2\text{Se}_3]$

As shown in Scheme 1, the prolonged thermolysis reaction of $[\text{Cp}^*\text{NbCl}_4]$ with four equivalents of $\text{Li}[\text{BH}_2\text{Se}_3]$ led to the formation of brown solid **1** and green solid **2**. The ^1H NMR spectrum of **1** showed a single peak at $\delta = 2.21$ ppm, which suggests the existence of a single Cp* environment. On the other hand, the ^1H NMR spectrum of **2** showed two very close resonances that appeared at $\delta = 2.18$ ppm in a 2:1 ratio, which suggests the existence of two different Cp* environments. The presence of one and two Cp* environments in **1** and **2**, respectively, was further confirmed by $^{13}\text{C}\{^1\text{H}\}$ NMR spectra. In addition, broad chemical

shifts at $\delta = 3.87$ and 3.65 ppm in ^1H NMR of **1** and **2**, respectively, suggested the presence of terminal B–H protons in **1** and **2**. Moreover, the IR spectroscopy of **1** and **2** confirmed the existence of this terminal B–H proton. The $^{11}\text{B}\{^1\text{H}\}$ NMR spectrum of **1** showed a single resonance that appeared at $\delta = -8.3$ ppm, whereas a chemical shift at $\delta = -6.4$ ppm has been observed in the $^{11}\text{B}\{^1\text{H}\}$ NMR of **2**. The mass spectra of **1** and **2** showed peaks at m/z 1234.5158 and m/z 1312.4354, respectively. Further, single crystal X-ray diffraction analyses were carried out on suitable crystals, **1** and **2**, to confirm the spectroscopic assignments and to conclude their structures without any ambiguity.



Scheme 1. Synthesis of the trimetallic chalcogen-rich niobaboranes **1** and **2** (the μ -Se in cluster **1** and **2** are omitted for clarity).

The single crystal X-ray analyses revealed compounds **1** and **2** as the trimetallic species $[(\text{NbCp}^*)_3(\mu_3\text{-Se})_3(\text{BH})(\mu\text{-Se})_3]$ (**1**) (Figure 1a) and $[(\text{NbCp}^*)_3(\mu_3\text{-Se})_3(\mu\text{-Se})_3(\text{BH})(\mu\text{-Se})]$ (**2**) (Figure 1b), respectively. Both the trimetallic species consist of an equilateral Nb_3 triangular core. The Nb–Nb bond distances in **1** (3.270(2), 3.271(2) and 3.272(3) Å), and in **2** (3.254(5), and 3.307(4) Å) are comparable. They are slightly longer than those reported in other niobaboranes and niobaheteroboranes [50,53,55]. The internal angles ($\angle\text{Nb-Nb-Nb}$) of the triangular framework in **1** ($59.96(5)^\circ$, $59.99(5)^\circ$ and $60.05(5)^\circ$), and **2** ($58.94(10)^\circ$, and $60.53(5)^\circ$) are close to 60° . Six monoselenide atoms bridge all the edges of the Nb_3 -triangle in compounds **1** and **2**. In the case of **1**, the three selenide units are capped by a {BH} unit. Therefore, a selenaborate $[\text{Se}_3\text{BH}]^-$ ligand coordinates the triangular tri-niobium framework from the top in **1**. The B–Se bond distances of 2.095(18), 2.101(18), and 2.107(18) Å in **1** are comparable with those measured in the reported metallaheteroboranes [52,54]. Alternatively, the core geometry of **1** can also be viewed as a cubane-like cluster with one missing vertex, a niobium-selenium analogue of the trimetallic species $[(\text{TaCp}^*)_3(\mu_3\text{-S})_3(\text{BH})(\mu\text{-S})_3]$ [**1**] [51]. As three Nb–Nb bonds are present and one metal vertex is missing in **1**, the cluster valence electron count for trimetallic **1** must be $(80 - 18 - (3 \times 2)) = 56$; however, the actual electron count of **1** is $\{3(\text{NbCp}^*) + 3(\mu_3\text{-Se}) + 3(\mu\text{-Se}) + (\text{BH})\} = \{30 + 12 + 6 + 2\} = 50$. Therefore, cluster **1** is a hypo-electronic cluster. On the other hand, two of the bridging Se atoms of **2** are directly bonded to the boron atom, while the other selenium atom (Se5) is bridged between B1 and Se4 atoms in **2**. The B–Se and Se–Se bond distances of **2** are comparable with other reported B–Se and Se–Se single bonds. As the core geometry of tri-niobium species **2** can be generated by incorporating a selenium atom in between one of the B–Se bonds of cubane-type cluster **1**, trimetallic species **2** can be viewed as a homocubane-like cluster with one missing vertex, a selenium analogue of the trimetallic species $[(\text{NbCp}^*)_3(\mu_3\text{-S})_3(\mu\text{-S})_3(\text{BH})(\mu\text{-S})]$ (**1**) [53]. On the other hand, a C_3 axis passes through the BH unit and the midpoint of the Nb_3 triangle of **1**, which makes compound **1** a symmetric cluster, and its spectroscopic data positively corroborates with the X-ray structure. In addition, in line with the spectroscopic data, the solid-state structure of **2** exhibits a symmetry plane that passes through the $\text{Nb}1'$, B1, Se5, Se4 and the centre of the Nb1–Nb2 bond.

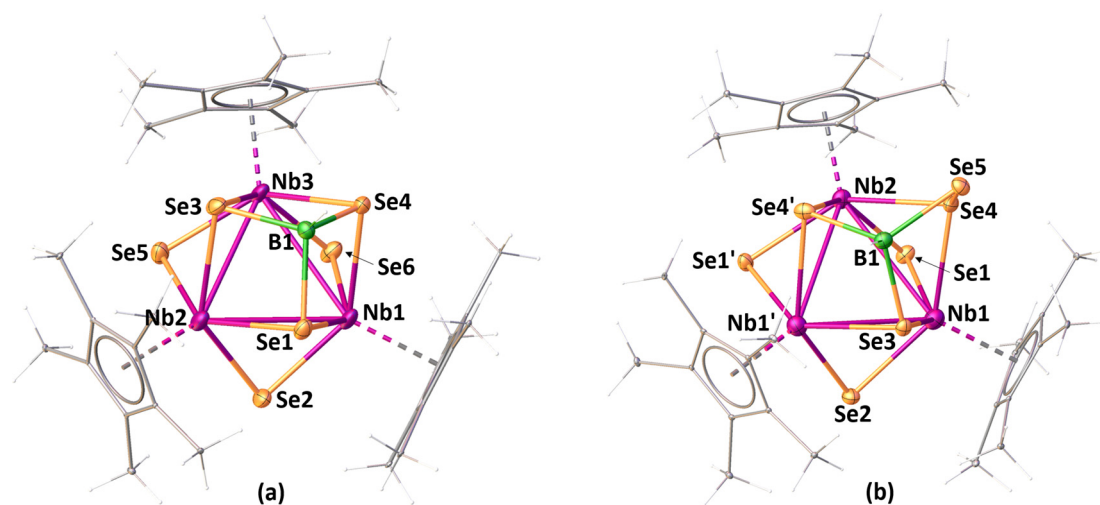
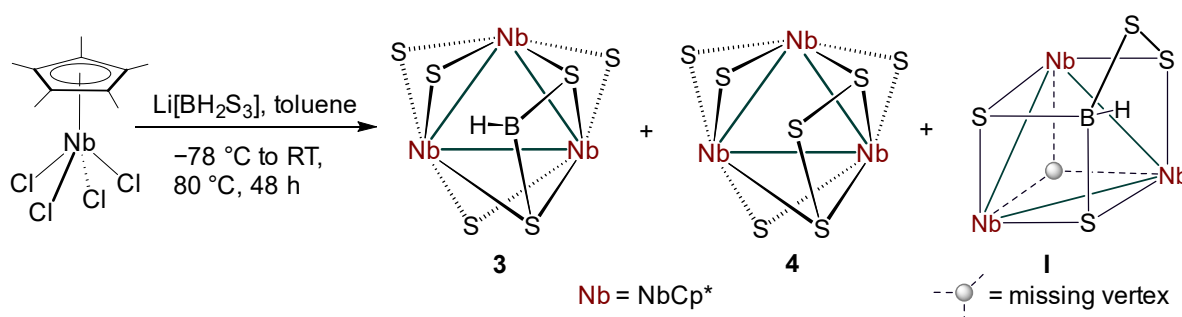


Figure 1. Molecular structures and labelling diagrams of **1** (a) and **2** (b). Selected bond lengths (Å) and angles (deg) in **1**: Nb1-Nb2 3.270(2), Nb1-Nb3 3.271(2), Nb2-Nb3 3.272(3), B1-Se3 2.07(3), B1-Se4 2.11(3), Nb1-Se1 2.672(3), Nb2-Se3 2.670(3); Nb1-Nb3-Nb2 59.96(5), Se1-B1-Se4 97.8(13), Nb1-Se1-Nb2 75.47(8); in **2**: Nb1-Nb1' 3.254(5), Nb1-Nb2 3.307(4), Nb1-Se4 2.669(4), Nb2-Se4 2.639(4), Se4-Se5 2.210(7), B1-Se5 2.07(3), B1-Se3 2.08(3); Nb1-Nb2-Nb1' 58.94(10), Nb1-Nb1'-Nb2 60.53(5), B1-Se5-Se4 86.4(17), Se3-B1-Se5 107.7(18), Nb2-Se4-Nb1 77.07(12).

2.2. Reactivity of $[\text{Cp}^*\text{NbCl}_4]$ with $\text{Li}[\text{BH}_2\text{S}_3]$

In order to isolate the sulfur analogue of **1**, we performed a thermolysis reaction of $[\text{Cp}^*\text{NbCl}_4]$ with four equivalents of $[\text{LiBH}_2\text{S}_3]$, for a prolonged time, which led to the formation of a yellow solid, as well as the known trimetallic homocubane-like cluster $[(\text{NbCp}^*)_3(\mu_3\text{-S})_3(\mu\text{-S})_3(\text{BH})(\mu\text{-S})]$ (**I**) (Scheme 2) [53]. The ^1H NMR spectrum of the yellow compound showed two ^1H resonances in a 2:1 ratio at $\delta = 2.10$ and 2.03 ppm, which suggests the presence of two different Cp^* environments. The presence of two different Cp^* environments was further confirmed by the $^{13}\text{C}\{^1\text{H}\}$ spectrum. Moreover, the ^1H NMR spectrum showed a peak at $\delta = 3.54$ ppm that suggested the presence of a terminal B-H proton. Further, the presence of the terminal B-H proton was confirmed by IR spectroscopy. In addition, the $^{11}\text{B}\{^1\text{H}\}$ NMR spectrum of the yellow compound showed a peak at $\delta = 3.8$ ppm. The mass spectrum showed molecular ion peaks at m/z 876.9071 and m/z 908.8798. However, these spectroscopic data were puzzling for forming a conclusion about the molecular structure. Thus, we have carried out single crystal X-ray diffraction analyses on a suitable yellow crystal to elucidate the solid-state structure.



Scheme 2. Synthesis of the chalcogen-rich niobaborane (**3**) and trimetallic polychalcogenide (**4**) species (the $\mu\text{-S}$ in cluster **I** is omitted for clarity).

Surprisingly, the single crystal X-ray analyses revealed the yellow crystal as a co-crystal of two inseparable solids (**3** and **4**). As shown in Figure 2, compounds **3** and **4** are the trimetallic species $[(\text{NbCp}^*)_3(\mu\text{-S})_4\{\mu\text{-S}_2(\text{BH})\}]$ and $[(\text{Cp}^*\text{Nb})_3(\mu\text{-S})_4\{\mu\text{-S}_2(\text{S})\}]$, respectively.

Both species **3** and **4** have an equilateral Nb₃ triangular core geometry. The Nb-Nb bond distances of 3.242 and 3.006 Å in **3** and **4**, respectively, are slightly shorter, especially the latter, than those in **1** and **2**. The internal angles (\angle Nb-Nb-Nb) of the triangular framework in **3** and **4** (62.38° and 55.25°) are also close to 60°. All the edges of the Nb₃-triangle in **3** and **4** are bridged by six mono-sulfide atoms. Further, two of these mono-sulfide atoms in **3** and **4** are bridged by {BH} and another by mono-sulfide units, respectively. Compound **4** is the Cp* analogue of [(NbCp⁺)₃(μ-S)₄{μ-S₂(S)}] (Cp⁺ = η⁵-C₅Me₄Et) reported earlier [56]. On the other hand, the thioborane unit {BS₂H} that coordinates two of the edges of the triangular tri-niobium framework from the top in **3** is quite unique. The B-S bond distances of 2.18(3) and 2.23(3) Å in **3** are slightly longer than those reported in the other metallaheteroboranes [38]. Interestingly, the thioborane unit also forms a tetratomic nonplanar metallathio boron cycle (Nb2-S1-B1-S4') with one of the Nb atoms. The X-ray structures of **3** and **4** corroborate well with their combined spectroscopic data. For example, ¹¹B{¹H} chemical shifts at δ = 3.8 ppm and ¹H chemical shift at δ = 3.54 ppm correspond to the {BH} unit of **3**. On the other hand, the ¹H chemical shifts correspond to the Cp* ligands of **3** and **4**; these should each appear as a 2:1 ratio for three Cp* ligands, as the symmetry plane passes through an Nb2 vector and the centre of the Nb1-Nb2' bond in **3**, and an Nb1 vector and the centre of the Nb2-Nb2' bond in **4**. However, in the combined ¹H NMR spectrum of **3** and **4**, these peaks for Cp* ligands accidentally overlapped and appeared in a 4:2; i.e., 2:1 ratio.

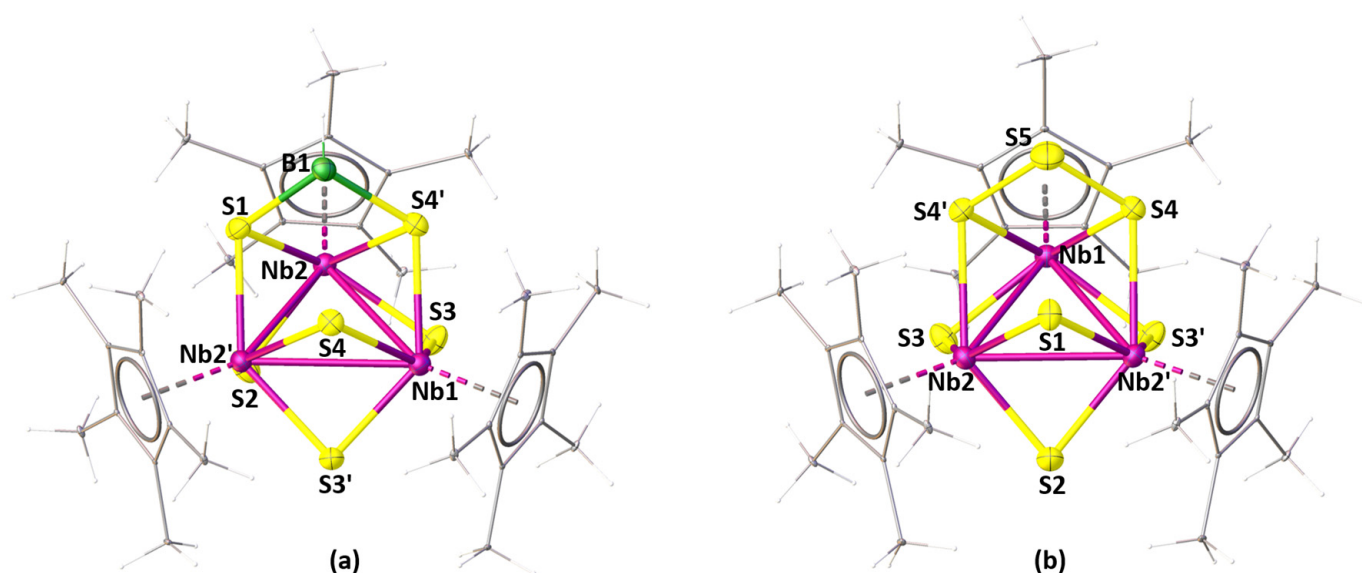


Figure 2. Molecular structures and labelling diagrams of **3** (a) and **4** (b). Selected bond lengths (Å) and angles (deg) in **3**: Nb1-Nb2 3.242, Nb2-Nb2' 3.006, Nb1-S4' 2.532(2), Nb2-S1 2.412(2), S1-B1 2.23(3), S4'-B1 2.18(3); Nb2'-Nb2-Nb1 62.38, Nb2-Nb1-Nb2' 55.25, Nb1-S4'-Nb2 77.51(6), S4'-B1-S1 94.0(11); in **4**: Nb1-Nb2 3.242, Nb2-Nb2' 3.006, Nb2-S4' 2.644(2), Nb1-S4 2.532(2), S4-S5 2.093(3); Nb2-Nb1-Nb2' 55.25, Nb2-S1-Nb2' 77.08(10), S4-S5-S4' 93.46(18).

2.3. Electronic Structural and Bonding Analysis of 1–4

To gain some insight into the bonding and electronic structures of **1–4**, we performed density functional theory (DFT) calculations at the BP86/def2-svp level of the theory [57,58]. Interestingly, the molecular orbital (MO) analyses showed that the HOMOs of **1–4** are mainly made of *d*-orbitals of the three Nb atoms, which overlap with each other and fully delocalize over the whole of the triangular trimetallic framework (Figure 3), illustrating 2-electron-3-centre bonding. Further, NBO [59–61] analyses were carried out to investigate more precisely the bonding in the Nb₃ triangle. The WBIs [62] of 0.362, and 0.365 in **1**; 0.324, and 0.381 in **2**; 0.355, and 0.467 in **3**; and 0.331, and 0.532 in **4** further support bonding interactions between Nb atoms within these species to form a Nb₃ tri-

angular skeleton. As shown in Chart 1, these types of trimetallic molecules show σ or π -aromaticity. This prompted us to probe the delocalized bonding in the Nb₃ core of 1–4. Thus, we employed the nucleus independent chemical shift (NICS) approach [21,22] for assessing the aromaticity of clusters 1–4. The NICS(0) (the negative of the isotropic magnetic shielding at the centre of the Nb₃ ring) for 1–4 were found to be –16.8, –20.3, –17.7, and –21.0 ppm, respectively, with negative numbers indicating aromaticity. In addition, the NICS(0)_{zz} values of 1–4, –48.1, –46.8, –45.7, and –47.5, respectively, quantify the out of the plane aromaticity. The NICS(0.5), NICS(–0.5), NICS(1), and NICS(–1) values computed for 1–4 are also negative, which show a ring current, indicating the presence of induced diatropic ring currents, which typically suggests three-dimensional aromaticity (Table S1, see Supplementary Materials). Therefore, the existence of an aromatic system plays a key role in the stabilization of 1–4.

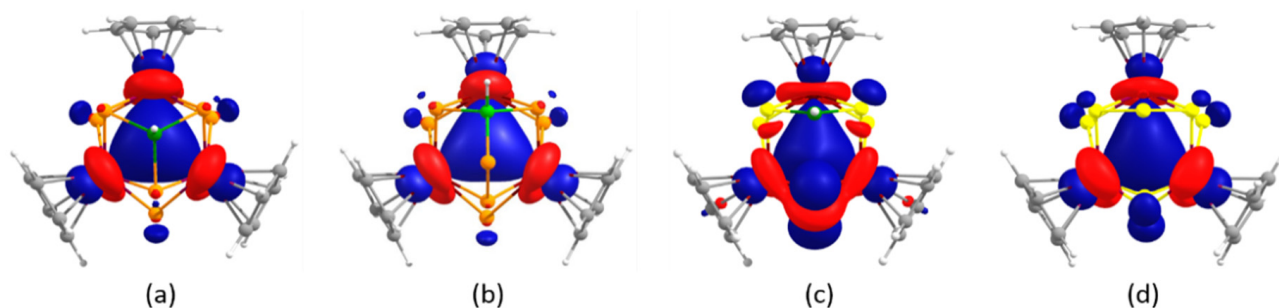


Figure 3. (a) HOMO of 1, (b) HOMO of 2, (c) HOMO of 3, and (d) HOMO of 4 depicting bonding within triangular Nb₃ frameworks. (Contour values for isosurface = ± 0.04 [e/bohr³]^{1/2}).

The triangular trimetallic skeleton of 1–4 further captured borate, borane, and chalcogen units. Therefore, we further analyzed the way they bind together. An MO analysis of 1 showed significant orbital overlap interaction between the triangular Nb₃ framework and the selenaborate {Se₃BH}[–] ligand, which is depicted in HOMO-3, HOMO-6, HOMO-7, and HOMO-8 (Figures 4a and S13). Further, an NBO analysis depicted the strong B-Se bonding interaction within the selenaborate {Se₃BH}[–] ligand in 1, which is further supported by WBI (0.887, 0.887, and 0.883) for B-Se interactions. With the exception of the bonding scenario along B1-Se7 and Se7-Se5, similar types of bonding interactions were observed in the MO (Figures 4d and S14) and NBO (Figure 4e) analyses of 2. WBIs of 1.064 and 0.909 support the strong bonding interaction between B1-Se and Se7-Se5, respectively. Further, a natural charge analysis of 1 and 2 showed that the three Nb atoms and the B atom act as acceptors, whereas the Se atoms act as donors (Table S2). On the other hand, the MO analyses of 3 and 4 showed significant orbital overlap interaction in the triangular Nb₃ framework and the directly connected six S atoms (Figures S15 and S16). In addition, substantial orbital overlap interactions among the p-orbitals of two of these directly metal-connected chalcogens and {BH} unit of 3, and mono-sulfur unit of 4, are depicted in HOMO-23 (3), and HOMO-8 (4), respectively (4(g) and Figure S16). In addition, an NBO analysis also illustrates the S-B bonding interaction in 3 (Figure 4h), which is also supported by higher WBIs (Table S3). Additionally, the Laplacian plot of electron density [63–65] showed areas of charge concentration, BCPs, and bond paths between B-Se in 1 (Figure 4c), B-Se and Se-Se in 3 (Figure 4f), S-B in 3 (Figure 4i), and S and S in 4 (Figure S17). Finally, the HOMO-LUMO energy gap in 2 (1.224 eV) is relatively smaller than those in 1 (1.296 eV), 3 (1.467 eV), and 4 (1.402 eV).

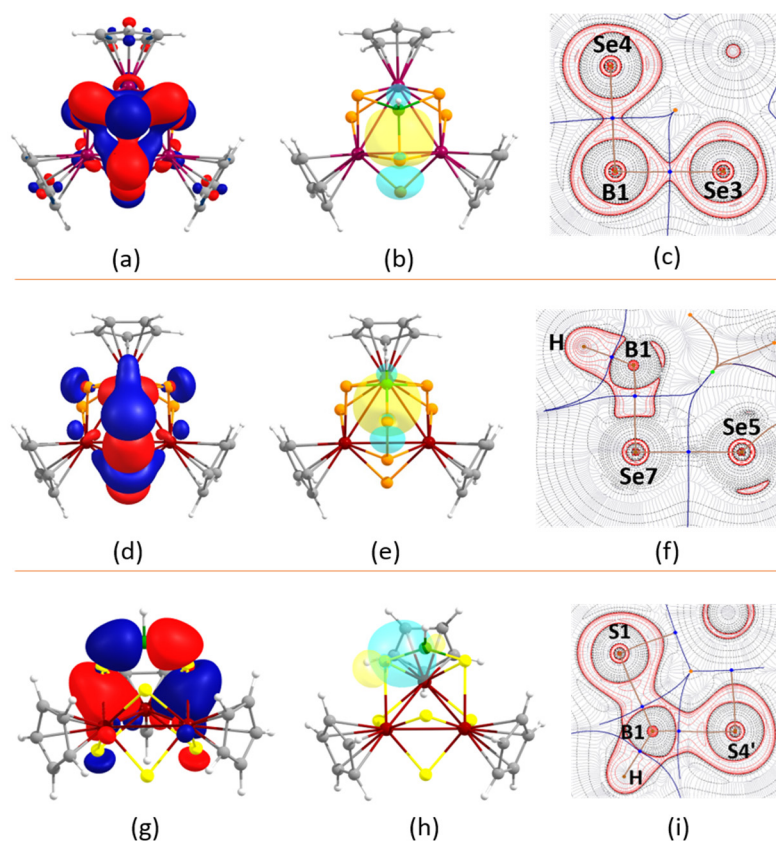


Figure 4. Investigation of the B-Se, Se-Se, and B-S bonding of **1**, **2**, and **3**, respectively. (a) HOMO-6 of **1**, (b) NBO depicting the B-Se bonding interaction in **1**, (c) contour-line diagrams of the Laplacian of electron density in the Se3-B1-Se4 plane of **1**, (d) HOMO-26 of **2**, (e) NBO depicting the B-Se bonding interaction in **2**, (f) contour-line diagrams of the Laplacian of electron density in the B1-Se7-Se5 plane of **2**, (g) HOMO-23 of **3**, (h) NBO depicting the B-S bonding interaction in **3**, (i) contour-line diagrams of the Laplacian of electron density in the S1-B1-S4' plane of **3**. In the contour-line diagrams of the Laplacian of electron density, solid red lines indicate areas of charge concentration [$\nabla^2\rho(r) < 0$], while dashed black lines show areas of charge depletion [$\nabla^2\rho(r) > 0$]. Blue dots indicate bond critical points (BCPs), and the brown line depicts the bond paths. (Contour values for isosurface = ± 0.04 [e/bohr³]^{1/2}).

3. Materials and Methods

All manipulations were carried out under an inert atmosphere of argon, either inside a glove box or by making use of standard Schlenk line techniques. All of the solvents were dried and distilled before use, employing standard literature procedures. [Cp*NbCl₄] [66], Li[BH₂E₃] (E = S and Se) [67,68], and the external reference used for analyzing ¹¹B{¹H} NMR, [Bu₄N(B₃H₈)], were all prepared in accordance with reported procedures [69]. [LiBH₄·THF], S powder, and Se powder (Merck KGaA, Darmstadt, Germany) were employed as received. The reaction mixtures were separated by performing thin layer chromatography using aluminum-supported silica gel TLC plates (Merck KGaA, Darmstadt, Germany) of 250 μm diameter. A 500 MHz Bruker FT-NMR spectrometer (Bruker, Billerica, MA, USA) was used to record ¹H, ¹¹B{¹H}, and ¹³C NMR spectra. The residual solvent protons were taken as a reference (CDCl₃, δ = 7.26 ppm), whereas a [D₆] benzene solution of [Bu₄N(B₃H₈)], taken in a sealed tube, was used as an external reference (δ_B = −30.07 ppm) for analyzing ¹¹B{¹H} NMR spectra. A Bruker MicroTOF-II mass spectrometer (Bruker Daltonics, Bremen, Germany) was used to record ESI mass spectra. IR spectra were recorded with a JASCO FT/IR-1400 spectrometer (JASCO, Easton, PA, USA). It is important to note

that elemental analysis of these compounds could not be performed due to low yields and higher sensitivity.

3.1. Synthesis of 1 and 2

A suspension of Cp*NbCl₄ (0.20 g, 0.54 mmol) in 20 mL of toluene was made in a flame-dried Schlenk tube. A freshly prepared solution of Li[BH₂Se₃] (2.16 mmol) in THF was added to the toluene suspension. The reaction mixture was stirred and heated at 80 °C for 48 h. The solvent was dried by applying a vacuum, and the residue was extracted into an *n*-hexane/CH₂Cl₂ mixture (80:20 *v/v*) and passed through Celite. After removing the volatiles by applying a vacuum, chromatographic separation of the residue was carried out using TLC plates. Elution with a *n*-hexane/CH₂Cl₂ mixture (70:30 *v/v*) formed brown solid **1** (0.023 g, 11% yield) and green solid **2** (0.027 g, 12% yield).

Spectroscopic data of **1**: MS (ESI⁺): *m/z* calculated for C₃₂NH₄₈Nb₃Se₆BNa⁺ [(M – H) + Na + CH₃CN]⁺: 1234.6009, found: 1234.5158. ¹¹B{¹H} NMR (160 MHz, CDCl₃, 22 °C): δ = –8.3 ppm; ¹H NMR (500 MHz, CDCl₃, 22 °C): δ = 2.21 (s, 45 H; 3 × Cp*), 3.87 ppm (b, B–H_t); ¹³C{¹H} NMR (125 MHz, CDCl₃, 22 °C): δ = 14.7 (C₅Me₅), 117.9 ppm (C₅Me₅); IR (CH₂Cl₂, cm^{–1}): 2515 (B–H_t).

Spectroscopic data of **2**: MS (ESI⁺): *m/z* calculated for C₃₀H₄₇Nb₃Se₇NaKH⁺ [M + Na + K + H]⁺: 1312.4714, found: 1312.4354. ¹¹B{¹H} NMR (160 MHz, CDCl₃, 22 °C): δ = –6.4 ppm; ¹H NMR (500 MHz, CDCl₃, 22 °C): δ = 2.18 (s, 15H; 1 × Cp*), 2.18 ppm (s, 30H; 2 × Cp*), 3.65 ppm (b, B–H_t); ¹³C{¹H} NMR (125 MHz, CDCl₃, 22 °C): δ = 14.3 (C₅Me₅), 14.8 (C₅Me₅), 116.9 (C₅Me₅), 117.8 ppm (C₅Me₅); IR (CH₂Cl₂, cm^{–1}): 2489 (B–H_t).

3.2. Synthesis of 3 and 4

Under similar experimental conditions, a reaction of Li[BH₂S₃] (2.16 mmol) with Cp*NbCl₄ (0.20 g, 0.54 mmol) was carried out. The solvent was dried by applying a vacuum, and the residue was extracted into an *n*-hexane/CH₂Cl₂ mixture (80:20 *v/v*) and passed through Celite. After removing the volatiles by applying a vacuum, chromatographic separation of the residue was carried out using TLC plates. Elution with *n*-hexane/CH₂Cl₂ mixture (70:30 *v/v*) formed a mixture of **3** and **4** as a yellow solid (0.026 g, 16% yield) along with a known orange solid [(NbCp*)₃(μ₃-S)₃(μ-S)₃(BH)(μ-S)] [**53**] (0.015 g, 9% yield).

Combined spectroscopic data of **3** and **4**: MS (ESI⁺): *m/z* calculated for C₃₀H₄₆Nb₃S₆⁺ [M – BH + H]⁺: 876.9115, found: 876.9071; *m/z* calculated for C₃₀H₄₆Nb₃S₇⁺ [M + H]⁺: 908.8836, found: 908.8798. ¹¹B{¹H} NMR (160 MHz, CDCl₃, 22 °C): δ = 3.8 ppm; ¹H NMR (500 MHz, CDCl₃, 22 °C): δ = 2.03 (s, 30 H; 2 × Cp*), 2.10 (s, 60 H; 4 × Cp*), 3.54 ppm (b, B–H_t); ¹³C{¹H} NMR (125 MHz, CDCl₃, 22 °C): δ = 12.9 (C₅Me₅), 13.1 (C₅Me₅), 116.9 (C₅Me₅), 119.0 (C₅Me₅); IR (CH₂Cl₂, cm^{–1}): 2472 (B–H_t).

3.3. X-ray Structure Determination

A Bruker AXS Kappa APEX-II CCD diffractometer (Bruker AXS Inc., Madison, WI, USA) bearing a graphite monochromated MoK_α (λ = 0.71073 Å), radiated at 296 K, was used to collect and integrate the crystal data of compounds **1**–**5**. Heavy atom methods were employed to solve the structures by making use of SHELXS-97 or SIR92, and structure refinement was achieved using SHELXL-2018/3 [70–72]. Structures of the molecules were drawn with Olex2 [73]. Note that all atoms of the disordered component of **1** were found to have shifted by the same vector (0.3958, –0.2374, 0.0078) as the corresponding atoms of the main molecule. This showed the disorder component to be a translation of the main molecule through a distance of 6.631 Å in the direction of the vector (0.3958, –0.2374, 0.0078). The Cp* and the boron atoms of the main molecule were moved through this vector in a separate job. These atoms' cards were then copied and put in the main res file, relabeled and assigned the occupancies –21.0 The Cp* and boron atoms became correctly attached to the disorder component. The molecules were refined with suitable restraints. As the scattering strength of the carbon atoms of the minor disordered component is only 6/20 = 0.3 e, the restraints were needed for refinement. Note that multiple recrystallizations

of **2** from various solvents provided extremely thin crystals, which diffracted poorly. Thus, R_{int} is high for **2**. However, proper analysis of the X-ray data provided conclusive proof of the structure, which also positively corroborated with the other spectroscopic evidence. In addition, the atoms Se5 and B1 had 50% occupancy only and of the bonds Se5-B1 and Se5'-B1', any one of them only existed in a given molecule. Compound **2** crystallized along with the CHCl_3 solvent molecule. Compounds **3** and **4** are a 50:50 mixture of a yellow co-crystal and crystallized along with two CH_2Cl_2 solvent molecules, whereas The Cambridge Crystallographic Data Centre has been provided with the crystallographic data of the compounds with supplementary publication no. CCDC-2203605 (**1**), 2203607 (**2**), and 2203609 (**3** and **4**).

Crystal data of **1**: $[\text{C}_{30}\text{H}_{46}\text{BNb}_3\text{Se}_6]$, $M_r = 1169.97$, triclinic, $P\bar{1}$, $a = 11.984(2)$ Å, $b = 11.986(2)$ Å, $c = 15.488(3)$ Å, $\alpha = 98.184(8)^\circ$, $\beta = 98.597(9)^\circ$, $\gamma = 119.817(7)^\circ$, $V = 1846.7(6)$ Å³, $Z = 2$, $\rho_{\text{calc}} = 2.104$ g/cm³, $\mu = 6.848$ mm⁻¹, $F(000) = 1116.0$, $R_1 = 0.0884$, $wR_2 = 0.2140$, 5681 independent reflections, $[2\theta \leq 48.792]$ and 727 parameters.

Crystal data of **2**: $2[\text{C}_{30}\text{H}_{46}\text{B}_1\text{Nb}_3\text{Se}_7] + [\text{CHCl}_3]$, $M_r = 2617.22$, orthorhombic, $Cmc2_1$, $a = 15.792(3)$ Å, $b = 16.816(3)$ Å, $c = 16.237(2)$ Å, $\alpha = 90^\circ$, $\beta = 90^\circ$, $\gamma = 90^\circ$, $V = 4312.0(12)$ Å³, $Z = 2$, $\rho_{\text{calc}} = 2.016$ g/cm³, $\mu = 6.805$ mm⁻¹, $F(000) = 2484.0$, $R_1 = 0.0739$, $wR_2 = 0.1494$, 3944 independent reflections, $[2\theta \leq 49.998]$ and 235 parameters.

Crystal data of **3** and **4**: $[\text{C}_{30}\text{H}_{46}\text{BS}_6\text{Nb}_3] + [\text{C}_{30}\text{H}_{45}\text{S}_7\text{Nb}_3] + 2[\text{CH}_2\text{Cl}_2]$, $M_r = 1090.48$, orthorhombic, $Pnma$, $a = 16.903(3)$ Å, $b = 16.437(3)$ Å, $c = 15.215(3)$ Å, $\alpha = \beta = \gamma = 90^\circ$, $V = 4227.3(14)$ Å³, $Z = 4$, $\rho_{\text{calc}} = 1.713$ g/cm³, $\mu = 1.422$ mm⁻¹, $F(000) = 2200$, $R_1 = 0.0546$, $wR_2 = 0.1606$, 3857 independent reflections, $[2\theta \leq 49.998]$ and 232 parameters.

3.4. Computational Details

All molecules were fully optimized using the BP86 functional [57,58], in conjunction with a def2-svp basis set using the *Gaussian 09* program (Gaussian, Wallingford, CT, USA) [74]. All compounds were fully optimized in gaseous state using their X-ray crystallographic structures. The calculations were performed with the Cp analogues, instead of Cp*, to save computing time. Note that the B1...S4 distance of **3** was frozen and optimized. Further, frequency calculations of **3** confirmed the absence of any imaginary frequency. NBO analyses were carried out with the NBO partitioning scheme [59–61] as employed in *Gaussian 09*. Wiberg bond indexes (WBI) [62] were obtained from the NBO analysis. QTAIM analyses [63–65] were performed utilizing the *Multiwfn* V.3.6 package (Multiwfn, Beijing, China) [75]. The aromaticity of the compounds was evaluated by calculating the Nucleus Independent Chemical Shift (NICS) indices [21,22] on the optimized geometries, at the same level of theory, by using the GIAO method implemented in *Gaussian*. All the optimized structures and orbital graphics were produced using *Gaussview* [76] and *Chemcraft* [77].

4. Conclusions

In summary, we have synthesized and structurally characterized novel species containing a 2-electron aromatic tri-niobium skeleton, which further stabilizes different types of main group units, such as borate, borane, and mono/di-chalcogenide units. The common cluster core of all these novel species is Nb_3E_6 ($\text{E} = \text{S}, \text{Se}$). Theoretical calculations revealed the participation of Nb d-orbitals to form an aromatic Nb_3 framework. In addition, the pivotal role of the aromatic Nb_3 skeleton in the stabilization of borate, borane, and mono/di-chalcogenide units is revealed. Additional exploration to evaluate the scope for isolation of the other main group units, utilizing the trimetallic skeleton of group 4 and 5 transition metals, is currently underway.

Supplementary Materials: The following supporting information can be downloaded at: <https://www.mdpi.com/article/10.3390/molecules27217473/s1>, Figures S1–S12: spectroscopic details of 1–4; Figures S13–S16: selected molecular orbitals of 1–4, Figure S17: contour-line diagrams of the Laplacian of electron density of 4, Figures S18–S21: Optimized geometries of 1–4, Tables S1–S3: NICS values, calculated natural charges and natural valence population, and WBIs of 1–4. Application of the linear; [78–81].

Author Contributions: Conceptualization, S.K., S.G. and J.-F.H.; methodology, S.K., S.G. and J.-F.H.; software, S.K. and D.C.; validation, S.G. and J.-F.H.; formal analysis, S.K. and D.C.; investigation, S.K. and D.C.; data curation, S.K. and D.C.; writing—original draft preparation, S.K., S.G. and J.-F.H.; writing—review and editing, S.G. and J.-F.H.; visualization, S.K. and D.C.; supervision, S.G. and J.-F.H.; project administration, S.G. and J.-F.H.; funding acquisition, S.G. All authors have read and agreed to the published version of the manuscript.

Funding: This work was supported by the SERB, Grant No. CRG/2019/001280, New Delhi, India and the Centre of Excellence on Molecular Materials and Functions under the Institution of Eminence scheme of IIT Madras.

Institutional Review Board Statement: Not applicable.

Informed Consent Statement: Not applicable.

Data Availability Statement: Supporting data reported can be found as Supplementary Materials.

Acknowledgments: S.K. and D.C. thank IIT Madras for research fellowships. We thank P.K. Sudhadevi Antharjanam, Babu Varghese, V. Ramkumar, and SAIF, IIT Madras for single-crystal X-ray data collection and structure analyses. Computational facilities of IIT Madras are gratefully acknowledged.

Conflicts of Interest: The authors declare no conflict of interest.

Sample Availability: Samples of the compounds are available from the authors upon request.

References and Note

1. Liddle, S.T. *Molecular Metal–Metal Bonds: Compounds, Synthesis, Properties*; Wiley-VCH: London, UK, 2015. [CrossRef]
2. Wang, X.-B.; Wang, L.-S. Probing the Electronic Structure and Metal–Metal Bond of $\text{Re}_2\text{Cl}_8^{2-}$ in the Gas Phase. *J. Am. Chem. Soc.* **2000**, *122*, 2096–2100. [CrossRef]
3. Roy, D.K.; Ghosh, S. Group 5 Metal–Metal Bonds. In *Molecular Metal–Metal Bonds: Compounds, Synthesis, Properties*; Liddle, S., Ed.; Wiley-VCH: London, UK, 2015; Chapter 5; pp. 91–138.
4. Le Guennic, B.; Jiao, H.; Kahlal, S.; Saillard, J.-Y.; Halet, J.-F.; Ghosh, S.; Beatty, A.M.; Rheingold, A.L.; Fehlner, T.P. Synthesis and Characterization of Hypoelectronic Rhenaboranes. Analysis of the Geometric and Electronic Structures of Species Following Neither Borane nor Metal Cluster Electron Counting Paradigms. *J. Am. Chem. Soc.* **2004**, *126*, 3203–3217. [CrossRef] [PubMed]
5. Zubarev, D.Y.; Averkiev, B.B.; Zhai, H.-J.; Wang, L.-S.; Boldyrev, A.I. Aromaticity and antiaromaticity in transition-metal systems. *Phys. Chem. Chem. Phys.* **2008**, *10*, 257–267. [CrossRef] [PubMed]
6. Kar, S.; Pradhan, A.N.; Ghosh, S. Polyhedral Metallaboranes and Metallacarboranes. In *Comprehensive Organometallic Chemistry IV*, 4th ed.; Parkin, G., Meyer, K., O'hare, D., Eds.; Elsevier: Amsterdam, The Netherlands, 2022; Volume 9, pp. 263–369. [CrossRef]
7. Kar, S.; Pradhan, A.N.; Ghosh, S. Metal-rich Metallaboranes: Clusters Containing Triply and Tetra Bridging Borylene and Boride Units. *Coord. Chem. Rev.* **2021**, *436*, 213796. [CrossRef]
8. Kar, S.; Bairagi, S.; Haridas, A.; Joshi, G.; Jemmis, E.D.; Ghosh, S. Hexagonal Planar $[\text{B}_6\text{H}_6]$ within a $[\text{B}_6\text{H}_{12}]$ Borate complex; Structure and Bonding of $[(\text{Cp}^*\text{Ti})_2(\mu-\eta^6:\eta^6\text{-B}_6\text{H}_6)(\mu\text{-H})_6]$. *Angew. Chem. Int. Ed.* **2022**, *61*, e202208293. [CrossRef]
9. Cotton, F.A.; Walton, R.A. Metal-metal multiple bonds in dinuclear clusters. In *Clusters. Structure and Bonding*; Springer: Berlin/Heidelberg, Germany, 1985; Volume 62, pp. 1–49. [CrossRef]
10. Vivó, D.G.; Ramos, A.; Ruiz, M.A. Cyclopentadienyl and related complexes of the group 6 elements having metal–metal triple bonds: Synthesis, structure, bonding and reactivity. *Coord. Chem. Rev.* **2013**, *257*, 2143–2191. [CrossRef]
11. Chisholm, M.H. Mixed valency and metal–metal quadruple bonds. *Coord. Chem. Rev.* **2013**, *257*, 1576–1583. [CrossRef]
12. Nguyen, T.; Sutton, A.D.; Brynda, M.; Fettingner, J.C.; Long, G.J.; Power, P.P. Synthesis of a Stable Compound with Fivefold Bonding Between Two Chromium(I) Centers. *Science* **2005**, *310*, 844–847. [CrossRef]
13. Doz, U.R.P.; Breher, F. To Boldly Pass the Metal–Metal Quadruple Bond. *Angew. Chem. Int. Ed.* **2006**, *45*, 3006–3010. [CrossRef]
14. Fehlner, T.P.; Halet, J.-F.; Saillard, J.-Y. *Molecular Clusters. A Bridge to Solid-State Chemistry*; Cambridge University Press: Cambridge, UK, 2007; pp. 85–138. [CrossRef]
15. Anju, R.S.; Saha, K.; Mondal, B.; Dorcet, V.; Roisnel, T.; Halet, J.-F.; Ghosh, S. Chemistry of Diruthenium Analogue of Pentaborane(9) with Heterocumulenes: Towards Novel Trimetallic Cubane-type Clusters. *Inorg. Chem.* **2014**, *53*, 10527–10535. [CrossRef]

16. Okamura, R.; Tada, K.; Matsubara, K.; Oshima, M.; Suzuki, H. Novel Trinuclear Trihydride Complexes of Ruthenium Having a Triply Bridging Borylene Ligand, $\{(\eta^5\text{-C}_5\text{Me}_5)\text{Ru}\}_3(\mu\text{-H})_3(\mu_3\text{-BX})$ ($X = \text{H, CN, OMe, OEt}$). Synthesis, Structure Determination, and Reaction with Benzothiophene. *Organometallics* **2001**, *20*, 4772–4774. [[CrossRef](#)]
17. Takao, T.; Suwa, H.; Okamura, R.; Suzuki, H. Formation of a Boraruthenacyclopentenyl Skeleton via B–C Bond Formation across a Triruthenium Plane. *Organometallics* **2012**, *31*, 1825–1831. [[CrossRef](#)]
18. Arnold, N.; Braunschweig, H.; Dewhurst, R.D.; Ewing, W.C. Unprecedented Borane, Diborane(3), Diborene, and Borylene Ligands via Pt-Mediated Borane Dehydrogenation. *J. Am. Chem. Soc.* **2016**, *138*, 76–79. [[CrossRef](#)]
19. Mednikov, E.G.; Dahl, L.F. Syntheses, structures and properties of primarily nanosized homo/heterometallic palladium CO/PR₃-ligated clusters. *Philos. Trans. R. Soc. A* **2010**, *368*, 1301–1332. [[CrossRef](#)]
20. Bag, R.; Kar, S.; Saha, S.; Gomosta, S.; Raghavendra, B.; Roisnel, T.; Ghosh, S. Heterometallic Triply-Bridging Bis-Borylene Complexes. *Chem. Asian J.* **2020**, *15*, 780–786. [[CrossRef](#)]
21. Chen, Z.; Wannere, C.S.; Corminboeuf, C.; Puchta, R.; Schleyer, P.v.R. Nucleus-independent chemical shifts (NICS) as an aromaticity criterion. *Chem. Rev.* **2005**, *105*, 3842–3888. [[CrossRef](#)]
22. Tsipis, C.A. Aromaticity/antiaromaticity in “bare” and “ligand-stabilized” rings of metal atoms. In *Metal-Metal Bonding. Structure and Bonding*; Parkin, G., Ed.; Springer: Berlin/Heidelberg, Germany, 2010; Volume 136, pp. 217–274. [[CrossRef](#)]
23. King, R.B. Three-Dimensional Aromaticity in Polyhedral Boranes and Related Molecules. *Chem. Rev.* **2001**, *101*, 1119–1152. [[CrossRef](#)]
24. Wang, Y.; Deyris, P.-A.; Caneque, T.; Blanchard, F.; Li, Y.; Bigi, F.; Maggi, R.; Blanchard, S.; Maestri, G.; Malacria, M. A Simple Synthesis of Triangular All-Metal Aromatics Allowing Access to Isolobal All-Metal Heteroaromatics. *Chem. Eur. J.* **2015**, *21*, 12271–12274. [[CrossRef](#)]
25. Boldyrev, A.I. All-Metal Aromaticity and Antiaromaticity. *Chem. Rev.* **2005**, *105*, 3716–3757. [[CrossRef](#)]
26. Popov, I.A.; Pan, F.-X.; You, X.R.; Li, L.J.; Matito, E.; Liu, C.; Zhai, H.-J.; Sun, Z.-M.; Boldyrev, A.I. Peculiar All-Metal s-Aromaticity of the $[\text{Au}_2\text{Sb}_{16}]^{4-}$ Anion in the Solid State. *Angew. Chem. Int. Ed.* **2016**, *55*, 15344–15346. [[CrossRef](#)]
27. Boldyrev, A.I.; Wang, L.S. Beyond organic chemistry: Aromaticity in atomic clusters. *Phys. Chem. Chem. Phys.* **2016**, *18*, 11589–11605. [[CrossRef](#)] [[PubMed](#)]
28. Huang, X.; Zhai, H.J.; Kiran, B.; Wang, L.S. Observation of d-Orbital Aromaticity. *Angew. Chem. Int. Ed.* **2005**, *44*, 7251–7254. [[CrossRef](#)] [[PubMed](#)]
29. Zhai, H.J.; Averkiev, B.B.; Zubarev, D.Y.; Wang, L.S.; Boldyrev, A.I. δ Aromaticity in $[\text{Ta}_3\text{O}_3]^-$. *Angew. Chem. Int. Ed.* **2007**, *46*, 4277–4280. [[CrossRef](#)] [[PubMed](#)]
30. Li, X.-W.; Pennington, W.T.; Robinson, G.H. A Metallic System with Aromatic Character. Synthesis and Molecular Structure of $\text{Na}_2[(\text{Mes}_2\text{C}_6\text{H}_3)\text{Ga}]_3$ ($\text{Mes} = 2,4,6\text{-Me}_3\text{C}_6\text{H}_2$): The First Cyclogallane. *J. Am. Chem. Soc.* **1995**, *117*, 7578–7579. [[CrossRef](#)]
31. Blanchard, S.; Fensterbank, L.; Gontard, G.; Lacote, E.; Maestri, G.; Malacria, M. Synthesis of Triangular Tripalladium Cations as Noble-Metal Analogues of the Cyclopropenyl Cation. *Angew. Chem. Int. Ed.* **2014**, *53*, 1987–1991. [[CrossRef](#)]
32. Robilotto, T.J.; Bacsa, J.; Gray, T.G.; Sadighi, J.P. Synthesis of a Trigold Monocation: An Isolobal Analogue of $[\text{H}_3]^+$. *Angew. Chem. Int. Ed.* **2012**, *51*, 12077–12080. [[CrossRef](#)]
33. Freitag, K.; Gemel, C.; Jerabek, P.; Oppel, I.M.; Seidel, R.W.; Frenking, G.; Banh, H.; Dilchert, K.; Fischer, R.A. The s-Aromatic Clusters $[\text{Zn}_3]^+$ and $[\text{Zn}_2\text{Cu}]$: Embryonic Brass. *Angew. Chem. Int. Ed.* **2015**, *54*, 4370–4374. [[CrossRef](#)]
34. Boronski, J.T.; Seed, J.A.; Hunger, D.; Woodward, A.W.; van Slageren, J.; Wooles, A.J.; Natrajan, L.S.; Kaltsoyannis, N.; Liddle, S.T. A crystalline tri-thorium cluster with σ -aromatic metal–metal bonding. *Nature* **2021**, *598*, 72–75. [[CrossRef](#)]
35. Braunschweig, H.; Dewhurst, R.D.; Gessner, V.H. Transition metal borylene complexes. *Chem. Soc. Rev.* **2013**, *42*, 3197–3208. [[CrossRef](#)]
36. Borthakur, R.; Saha, K.; Kar, S.; Ghosh, S. Recent advances in transition metal diborane(6), diborane(4) and diborene(2) chemistry. *Coord. Chem. Rev.* **2019**, *399*, 213021. [[CrossRef](#)]
37. Kaur, U.; Saha, K.; Gayen, S.; Ghosh, S. Contemporary developments in transition metal boryl complexes: An overview. *Coord. Chem. Rev.* **2021**, *446*, 214106. [[CrossRef](#)]
38. Saha, K.; Kaur, U.; Kar, S.; Mondal, B.; Joseph, B.; Antharjanam, P.K.S.; Ghosh, S. Trithia-diborinane and Bis(bridging-boryl) Complexes of Ruthenium Derived from a $[\text{BH}_3(\text{SCHS})]^-$ Ion. *Inorg. Chem.* **2019**, *58*, 2346–2353. [[CrossRef](#)]
39. Hosmane, N.S.; Maguire, J.A. Metallacarboranes of d- and f-block metals. In *Comprehensive Organometallic Chemistry III*, 3rd ed.; Crabtree, R.H., Mingos, D.M.P., Eds.; Elsevier: Amsterdam, The Netherlands, 2007; Volume 3, pp. 175–264. [[CrossRef](#)]
40. Kar, S.; Ghosh, S. Borane Polyhedra beyond Icosahedron. In *50th Anniversary of Electron Counting Paradigms for Polyhedral Molecules. Structure and Bonding*; Mingos, D.M.P., Ed.; Springer: Berlin/Heidelberg, Germany, 2021; Volume 187, pp. 109–138. [[CrossRef](#)]
41. De, A.; Zhang, Q.-F.; Mondal, B.; Cheung, L.F.; Kar, S.; Saha, K.; Varghese, B.; Wang, L.-S.; Ghosh, S. $[(\text{Cp}_2\text{M})_2\text{B}_9\text{H}_{11}]$ ($\text{M} = \text{Zr}$ or Hf): Early transition metal ‘guarded’ heptaborane with strong covalent and electrostatic bonding. *Chem. Sci.* **2018**, *9*, 1976–1981. [[CrossRef](#)]
42. Kar, S.; Bairagi, S.; Joshi, G.; Jemmis, E.D.; Ghosh, S. Metal stabilized $[\text{B}_8\text{H}_8]^{2-}$ derivatives with dodecahedral structure in solid- and solution-state: $[(\text{Cp}_2\text{MBH}_3)_2\text{B}_8\text{H}_6]$, ($\text{Cp} = \eta^5\text{-C}_5\text{H}_5$; $\text{M} = \text{Zr}$ (1-Zr) and Hf (1-Hf)). *Chem. Eur. J.* **2021**, *27*, 15634–15637. [[CrossRef](#)]

43. Roy, D.K.; Mondal, B.; Shankhari, P.; Anju, R.S.; Geetharani, K.; Mobin, S.M.; Ghosh, S. Supraicosahedral Polyhedra in Metallaboranes: Synthesis and Structural Characterization of 12-, 15- and 16-Vertex Rhodaboranes. *Inorg. Chem.* **2013**, *52*, 6705–6712. [[CrossRef](#)]
44. Mondal, B.; Bag, R.; Ghorai, S.; Bakthavachalam, K.; Jemmis, E.D.; Ghosh, S. Synthesis, Structure, Bonding and Reactivity of Metal Complexes comprising Diborane(4) and Diborene(2): $[(Cp^*Mo(CO)_2)_2\{\mu-\eta^2:\eta^2-B_2H_4\}]$ and $[(Cp^*M(CO)_2)_2B_2H_2M(CO)_4]$, $M=Mo,W$. *Angew. Chem. Int. Ed.* **2018**, *57*, 8079–8083. [[CrossRef](#)]
45. Saha, K.; Ghorai, S.; Kar, S.; Saha, S.; Halder, R.; Raghavendra, B.; Jemmis, E.D.; Ghosh, S. Stabilization of Classical $[B_2H_5]^-$: Structure and Bonding of $[(Cp^*Ta)_2(B_2H_5)(\mu-H)L_2]$ ($Cp^* = \eta^5-C_5Me_5$; $L = SCH_2S$). *Angew. Chem. Int. Ed.* **2019**, *58*, 17684–17689. [[CrossRef](#)]
46. Duff, A.W.; Jonas, K.; Goddard, R.; Kraus, H.J.; Krueger, C. The first triple-decker sandwich with a bridging benzene ring. *J. Am. Chem. Soc.* **1983**, *105*, 5479–5480. [[CrossRef](#)]
47. Rheingold, A.L.; Foley, M.J.; Sullivan, P.J. “Triple-decker sandwich” with a planar As_5 ring. Synthesis and crystal structure of $CpMo[\mu-(h^4-As_5)]MoCp$. *J. Am. Chem. Soc.* **1982**, *104*, 4727–4729. [[CrossRef](#)]
48. Herberich, G.E.; Hausmann, I.; Klaff, N. The 30-Electron Rule for Triple-Decker Complexes –Vanadium, Niobium and Tantalum Complexes as Illustrative Examples. *Angew. Chem. Int. Ed.* **1989**, *28*, 319–320. [[CrossRef](#)]
49. Bose, S.K.; Geetharani, K.; Varghese, B.; Ghosh, S. Unusual Organic Chemistry of a Metallaborane Substrate: Formation of Tantalaborane Complex with Bridging Acyl Group ($m-h^2$). *Inorg. Chem.* **2010**, *49*, 6375–6377. [[CrossRef](#)]
50. Brunner, H.; Gehart, G.; Nuber, B.; Wachter, J.; Ziegler, M.L. The Reaction of $[Cp^*_2Nb_2(B_2H_6)_2]$ ($Cp^* = \eta-EtMe_4C_5$) with Sulfur: Stabilization of the Tetrathioborato Ligand in Novel Sulfido Niobium Clusters. *Angew. Chem. Int. Ed.* **1992**, *31*, 1021–1023. [[CrossRef](#)]
51. Kawaguchi, H.; Tatsumi, K. Synthesis of (Pentamethylcyclopentadienyl)tantalum Sulfido Complexes via C–S Bond Cleavage of Triphenylmethanethiolate and Formation of a Novel Trithioborato Ligand. *Organometallics* **1997**, *16*, 307–309. [[CrossRef](#)]
52. Kar, S.; Saha, K.; Saha, S.; Bakthavachalam, K.; Dorcet, V.; Ghosh, S. Trimetallic Cubane-Type Clusters: Transition-Metal Variation as a Probe of the Roots of Hypoelectronic Metallaheteroboranes. *Inorg. Chem.* **2018**, *57*, 10896–10905. [[CrossRef](#)] [[PubMed](#)]
53. Kar, S.; Bairagi, S.; Saha, K.; Raghavendra, B.; Ghosh, S. Chalcogen stabilized trimetallic clusters: Synthesis, structures, and bonding of $[(Cp^*M)_3(E)_{6+m}(BH)_n]$ ($M = Nb$ or Ta ; $E = S$ or Se ; $m = 0$ or 1 or 2 ; $n = 0$ or 1). *Dalton Trans.* **2019**, *48*, 4203–4210. [[CrossRef](#)]
54. Saha, K.; Kar, S.; Ghosh, S. Chalcogen stabilized cubane-type cluster: Synthesis and structure of $[(Cp^*Ta)_3(\mu-Se)_3(\mu_3-Se)_3B(OBuCl)]$. *J. Indian Chem. Soc.* **2018**, *95*, 729–734. [[CrossRef](#)]
55. Bose, S.K.; Geetharani, K.; Ramkumar, V.; Mobin, S.M.; Ghosh, S. Fine Tuning of Metallaborane Geometries: Chemistry of Metallaboranes of Early Transition Metals Derived from Metal Halides and Monoborane Reagents. *Chem. Eur. J.* **2009**, *15*, 13483–13490. [[CrossRef](#)]
56. Leblanc, J.-C.; Moise, C.; Volpato, F.; Brunner, H.; Gehart, G.; Wachter, J.; Nuber, B. Comparative studies in the $Cp_2M(\eta^2-S_2)H$ series ($Cp = t-BuC_5H_4$, C_5MeEt ; $M = Nb, Ta$) on the reactivity of hydride and disulfide ligands. *J. Organomet. Chem.* **1995**, *485*, 237–242. [[CrossRef](#)]
57. Schmider, H.L.; Becke, A.D. Optimized density functionals from the extended G2 test set. *J. Chem. Phys.* **1998**, *108*, 9624–9631. [[CrossRef](#)]
58. Perdew, J.P. Density-functional approximation for the correlation energy of the inhomogeneous electron gas. *Phys. Rev. B* **1986**, *33*, 8822–8824. [[CrossRef](#)]
59. Glendening, E.D.; Reed, A.E.; Carpenter, J.E.; Weinhold, F. *NBO Program 3.1*; University of Wisconsin: Madison, WI, USA, 1988.
60. Reed, A.E.; Weinhold, F.; Curtiss, L.A. Intermolecular interactions from a natural bond orbital, donor-acceptor viewpoint. *Chem. Rev.* **1988**, *88*, 899–926. [[CrossRef](#)]
61. Weinhold, F.; Landis, R. *Valency and Bonding: A Natural Bond Orbital Donor-Acceptor Perspective*; Cambridge University Press: Cambridge, UK, 2005.
62. Wiberg, K.B. Application of the pople-santry-segal CNDO method to the cyclopropylcarbinyl and cyclobutyl cation and to bicyclobutane. *Tetrahedron* **1968**, *24*, 1083–1096. [[CrossRef](#)]
63. Bader, R.F.W. *Atoms in Molecules: A Quantum Theory*; Oxford University Press: Oxford, UK, 1990.
64. Bader, R.F.W. A Bond Path: A Universal Indicator of Bonded Interactions. *J. Phys. Chem. A* **1998**, *102*, 7314–7323. [[CrossRef](#)]
65. Bader, R.F.W. A quantum theory of molecular structure and its applications. *Chem. Rev.* **1991**, *91*, 893–928. [[CrossRef](#)]
66. Okamoto, T.; Yasuda, H.; Nakamura, A.; Kai, Y.; Kanehisa, N.; Kasai, N. Synthesis and Catalysis of Novel Mono- and Bis(diene) Complexes of Niobium and X-ray Structures of Binuclear $[Nb(\mu-Cl)(C_5H_5)(s-cis-butadiene)]_2$ and Mononuclear $Nb(C_5H_5)(s-cis-2,3-dimethylbutadiene)_2$. *J. Am. Chem. Soc.* **1988**, *110*, 5008–5017. [[CrossRef](#)]
67. Lalancette, J.M.; Frêche, A.; Monteux, R. Reductions with sulfurated borohydrides. I. Preparation of sulfurated borohydrides. *Can. J. Chem.* **1968**, *46*, 2754–2757. [[CrossRef](#)]
68. Lalancette, J.M.; Arnac, M. Reductions with sulfurated borohydrides. III. Borohydrides incorporating selenium and tellurium. *Can. J. Chem.* **1969**, *47*, 3695–3697. [[CrossRef](#)]
69. Ryschlewitsch, G.E.; Nainan, K.C.; Miller, S.R.; Todd, L.J.; Dewkett, W.J.; Grace, M.; Beall, H.; Hawthorne, M.F.; Leyden, R. Octahydrotriborate (1-)(B_3H_8) salt. *Inorg. Synth.* **1974**, *15*, 111–118. [[CrossRef](#)]
70. Sheldrick, G.M. *SHELXS-97*; University of Göttingen: Göttingen, Germany, 1997.

71. Altomare, A.; Cascarano, G.; Giacovazzo, C.; Guagliardi, A.; Burla, M.C.; Polidori, G.; Camalli, M. SIR92—A program for automatic solution of crystal structures by direct methods. *J. Appl. Crystallogr.* **1994**, *27*, 435–436. [[CrossRef](#)]
72. Sheldrick, G.M. Crystal structure refinement with SHELXL. *Acta Cryst.* **2015**, *C71*, 3–8. [[CrossRef](#)]
73. Dolomanov, O.V.; Bourhis, L.J.; Gildea, R.J.; Howard, J.A.K.; Puschmann, H.J. OLEX2: A complete structure solution, refinement and analysis program. *Appl. Crystallogr.* **2009**, *42*, 339–341. [[CrossRef](#)]
74. Frisch, J.M.; Trucks, G.W.; Schlegel, H.B.; Scuseria, G.E.; Robb, M.A.; Cheeseman, J.R.; Scalmani, G.; Barone, V.; Mennucci, B.; Petersson, G.A.; et al. *Gaussian 09, Revision C.01*; Gaussian, Inc.: Wallingford, CT, USA, 2010.
75. Lu, T.; Chen, F. Multiwfn: A multifunctional wavefunction analyzer. *J. Comput. Chem.* **2012**, *33*, 580–592. [[CrossRef](#)] [[PubMed](#)]
76. Dennington, I.I.; Keith, R.T.; Millam, J.; Eppinnett, K.; Hovell, W.L.; Gilliland, R. *GaussView, Version 3.09*; Semichem Inc.: Shawnee, KS, USA, 2003.
77. Zhurko, G.A. Available online: <https://www.chemcraftprog.com> (accessed on 24 April 2022).
78. ¹¹B{¹H} NMR spectra were processed with a backward linear prediction algorithm to eliminate the broad ¹¹B background signal of the NMR tube
79. Led, J.J.; Gesmar, H. Application of the linear prediction method to NMR spectroscopy. *Chem. Rev.* **1991**, *91*, 1413–1426. [[CrossRef](#)]
80. Yang, L.; Simionescu, R.; Lough, A.; Yan, H. Some observations relating to the stability of the BODIPY fluorophore under acidic and basic conditions. *Dyes Pigm.* **2011**, *91*, 264–267. [[CrossRef](#)]
81. Weiss, R.; Grimes, R.N. Sources of Line Width in Boron-11 Nuclear Magnetic Resonance Spectra. Scalar Relaxation and Boron-Boron Coupling in B₄H₁₀ and B₅H₉. *J. Am. Chem. Soc.* **1978**, *100*, 1401–1405. [[CrossRef](#)]